


Article

Effect of Pyrolysis Temperature on Removal Efficiency and Mechanisms of Hg(II), Cd(II), and Pb (II) by Maize Straw Biochar

Xuebo Hu ^{1,2,†}, Ruigang Zhang ^{3,†} , Bing Xia ^{1,2,4,5,*}, Rongrong Ying ^{4,5}, Zhewei Hu ^{4,5}, Xu Tao ¹, Hao Yu ¹, Fabao Xiao ¹, Qiaoying Chu ², Hongfeng Chen ^{1,2} and Jiazhong Qian ^{2,*}

- ¹ Anhui Provincial Academy of Eco-Environmental Science Research, Hefei 230071, China; huxuebo163@163.com (X.H.); tx829626@163.com (X.T.); ahhbyh@163.com (H.Y.); fabaoxiao@126.com (F.X.); chen71@163.com (H.C.)
- ² School of Resource and Environmental Engineering, Hefei University of Technology, Hefei 230009, China; cqy18355493373@163.com
- ³ School of Civil Engineering, Hefei University of Technology, Hefei 230009, China; zrgang@yeah.net
- ⁴ Nanjing Institute of Environmental Sciences, Ministry of Ecology and Environment, Nanjing 210042, China; yrr@nies.org (R.Y.); huzhewei@nies.org (Z.H.)
- ⁵ State Environmental Protection Key Laboratory of Soil Environmental Management and Pollution Control, Nanjing 210042, China
- * Correspondence: sweetblues@gmail.com (B.X.); qianjiazhong@hfut.edu.cn (J.Q.)
- † These authors contributed equally to this work.

Abstract: Pyrolysis temperature significantly affects the properties of biochar, which in turn can affect the removal of heavy metal ions and the underlying mechanism. In this work, biochars from the pyrolysis of maize straw at 300, 400, and 500 °C (BC300, BC400, and BC500, respectively) and wheat straw at 400 °C (WBC400) were investigated. The influence of production temperature on the adsorption of Hg²⁺, Cd²⁺, and Pb²⁺ by maize straw biochar was investigated by the characterization of the biochars and by adsorption tests. The adsorption capacities of maize and wheat straw biochar were compared in an adsorption experiment. Biochar BC400 showed the best physical and chemical properties and had the largest number of surface functional groups. The pseudo-second-order kinetic model was more suitable for describing the adsorption behavior of metal ions to biochar. The Langmuir model better fit the experimental data. Biochar BC400 had a higher adsorption speed and a stronger adsorption capacity than WBC400. The sorption of Pb²⁺ and Hg²⁺ to maize straw biochar followed the mechanisms of surface precipitation of carbonates and phosphates and complexation with oxygenated functional groups and delocalized π electrons. The adsorption mechanism for Cd²⁺ was similar to those of Hg²⁺ and Pb²⁺, but precipitation mainly occurred through the formation of phosphate. In the multi-heavy-metal system, the adsorption of Cd²⁺ by BC400 was inhibited by Pb²⁺ and Hg²⁺. In summary, BC400 biochar was most suitable for the adsorption effect of heavy metals in aqueous solution.

Keywords: production temperature; biochars; heavy metals; adsorption



Citation: Hu, X.; Zhang, R.; Xia, B.; Ying, R.; Hu, Z.; Tao, X.; Yu, H.; Xiao, F.; Chu, Q.; Chen, H.; et al. Effect of Pyrolysis Temperature on Removal Efficiency and Mechanisms of Hg(II), Cd(II), and Pb (II) by Maize Straw Biochar. *Sustainability* **2022**, *14*, 9022. <https://doi.org/10.3390/su14159022>

Academic Editors: Mingxiang Zhang, Zhenming Zhang and Jiakai Liu

Received: 26 March 2022

Accepted: 1 July 2022

Published: 22 July 2022

Publisher's Note: MDPI stays neutral with regard to jurisdictional claims in published maps and institutional affiliations.



Copyright: © 2022 by the authors. Licensee MDPI, Basel, Switzerland. This article is an open access article distributed under the terms and conditions of the Creative Commons Attribution (CC BY) license (<https://creativecommons.org/licenses/by/4.0/>).

1. Introduction

Heavy metal pollution of waterbodies has attracted considerable attention because of the accompanied toxic effects on flora, fauna, and humans, even at low concentrations [1,2]. Some of these effects are long-term effects caused by enrichment. Lead, cadmium, and mercury, which can harm human health [3], are largely present in the industrial wastewater of the mining industry, steel metallurgy, tanning, and pigment synthesis, as well as dye and petrochemical production [4], occurring as Pb²⁺, Cd²⁺, and Hg²⁺. Direct or indirect discharge into natural waterbodies can cause serious environmental and human health

problems, necessitating sustainable and effective methods for removing heavy metals from wastewater.

There have been many reports on the removal of heavy metals from wastewaters. The traditional technologies are ion exchange, electrochemical treatment, membrane separation, precipitation, and oxidation/reduction [5,6], but they are generally related to high processing costs, are not environmentally friendly, and are not suitable for large-scale applications [7]. As an alternative method, adsorption has significant advantages, such as high speed, availability, and efficiency [8,9]. Various adsorbents have been used for the removal of toxic heavy metals, including natural materials and synthetic composites, such as activated carbon graphene, modified cellulose, biochar, and nanocomposites [10]. However, the high manufacturing and regeneration costs of some adsorbents severely limit their large-scale application. Because of their high efficiency, low costs, and environmental safety, biochar adsorbents are widely used for heavy metal removal.

In recent years, biochar adsorbents have been successfully used to remove heavy metals from wastewater [11–13]. Previous studies compared the removal of Cd^{2+} from wastewater using biochar from three different biomass feedstocks (wood, cow dung, and crop straw) and found that crop straw biochar had the highest removal efficiency [14]. Biochar refers to carbon-rich residues of biomass pyrolyzed at low temperatures ($<700\text{ }^{\circ}\text{C}$) under oxygen-limited conditions [15]. According to previous studies, the biochar surface contains abundant functional groups (such as phenolic, hydroxyl, and carboxyl groups), has a high degree of porosity [16], and contains various minerals (e.g., N, S, Mg, K, Ca, and Na) [17]. The heavy metal removal mechanism of biochar is mainly attributed to the following mechanisms: cation exchange (e.g., Ca^{2+} , Mg^{2+} , and K^{+}), mineral precipitation (e.g., carbonate and phosphate), complexation with aerobic functional groups, and coordination with π electrons [18–20]. The adsorption capacity and mechanism of biochar depend on its characteristics, which in turn depend on the feedstock and production temperature [21]. A simple biochar can be generated from plant materials, such as husks, leaves, peels, stems, branches, and pods. The removal of heavy metal ions from an aqueous environment by the application of biochar from different biomass feedstocks has been reported previously [22]. Liu et al. studied the adsorption of Pb^{2+} using two biochars prepared from pinewood and rice husk and showed that pinewood biochar had a stronger adsorption ability than rice husk biochar [23].

Pyrolysis temperature plays a significant role in biochar formation, and biochar produced by pyrolysis at higher temperatures shows a more porous surface area and lower O/C and H/C ratios, resulting in a better adsorption effect for organic contaminants [24,25]. On the contrary, biochars produced at lower temperature not only save energy but also have better heavy metal adsorption effects in wastewater, mainly because they hold more oxygen-containing functional groups [26]. Therefore, selecting the appropriate pyrolysis temperature for biochar production is vital when the treatment of metal-contaminated wastewater is intended.

Numerous experimental studies have shown that the adsorption performance can be significantly improved through heat treatment or chemical treatment [21]. However, chemical treatment often results in a lower regeneration capability of the adsorbents, the production of toxic sludge, and increased processing costs. Wheat and maize are the most widely cultivated cereals in China, and most of the straws are left unused after harvest, thus wasting valuable resources [27]. In this context, biochar produced by low-temperature pyrolysis from wheat and maize straw is an economically feasible, potential heavy metal adsorbent. Currently, the adsorption mechanism for heavy metals in biochar is still in the exploration stage, and further studies are needed. In this study, biochar was obtained from maize and wheat straw, using three different pyrolysis temperatures. The objectives were as follows: (1) to determine the effect of pyrolysis temperature on removing Cd^{2+} , Hg^{2+} , and Pb^{2+} ; (2) to compare the heavy metal removal efficiencies of maize straw biochar with those of wheat straw biochar; (3) to reveal the mechanism underlying the removal of Cd^{2+} , Hg^{2+} , and Pb^{2+} in a multi-element system.

2. Materials and Methods

2.1. Biochar Production

Maize and wheat straw were obtained from Ma'anshan City, Anhui Province, China. Prior to pyrolysis, they were cleaned, air-dried, and cut into pieces of 10 cm. Subsequently, the biochar reactor was heated from room temperature to the target temperatures (300, 400, and 500 °C) at approximately 8.5 °C/min, and the target temperatures were maintained for about 10 h (Nanjing Zhironglian Technology Co., Ltd., Nanjing, China) until complete pyrolysis, after which the heating system was turned off, and the biochar was allowed to cool to room temperature. After pyrolysis, the biochar samples were ground in a mechanical jaw crusher, sieved through a 100-mesh screen, and stored in plastic bags for further characterization and sorption tests.

2.2. Biochar Characterization

The pH and electrical conductivity (EC) of the biochars were measured by pH and EC meters at a 1:10 biochar/water ratio after being equilibrated for 30 min and 24 h, respectively [28]. The ash content was determined using dry combustion at 800 °C for 4 h in a muffle furnace [29]. The elemental composition (C, H, and N) was measured using an elemental analyzer (Perkin Elmer, 2400 II, Waltham, MA, USA). The O content was estimated by mass difference: $O\% = 100 - (C\% + H\% + N\% + \text{Ash}\%)$ [30], and the N_2 -Brunauer–Emmett–Teller (BET) method was applied to analyze the specific surface area (SSA) using a surface area and porosity analyzer (Micromeritics Inc., USA). The total pore volume (TPV) was estimated via N_2 adsorption at $P/P_0 \sim 0.5$ [31], and the phosphorus concentration was determined using the molybdate/ascorbic acid colorimetric method [32]. Briefly, 5 g of biochar were placed into a 50 mL centrifuge tube with 50 mL of ultrapure water, mixed, and shaken at 25 °C for 30 min. Subsequently, the mixture was left to stand before being filtered, and the water-soluble phosphorus content of the biochar was determined.

The Fourier transformation infrared (FTIR) analysis was adopted to determine the composition of the functional groups. The FTIR spectra of the biochar samples were obtained with a Nicolet 170 SXTR infrared spectrometer and collected at 4000–400 cm^{-1} . The proportion of the biochars to spectroscopic-grade KBr was 1:200.

2.3. Sorption Tests

2.3.1. Adsorption Test Preparation

The designed heavy metal solutions were diluted from 2000 mg/L stock solutions of Hg^{2+} , Cd^{2+} , and Pb^{2+} , which were prepared in 0.01 mol/L NaNO_3 background ionic solution by dissolving analysis-grade HgCl_2 , $\text{Pb}(\text{NO}_3)_2$, and CdCl_2 , respectively. To ensure the best adsorption efficiency and prevent the formation of metal precipitation, the pH value of the background ionic solution was pre-adjusted to 5 using 0.1 mol/L HCl and 0.1 mol/L NaOH [33].

The adsorption tests were carried out in 50 mL polypropylene centrifuge tubes. Briefly, 0.125 g of biochar was mixed with 25 mL of heavy metal solution, shaken thoroughly, and equilibrated using end-over-end shaking at approximately 25 °C [31]. Subsequently, the mixtures were centrifuged at 3500 rpm for 10 min and filtered through 0.22 μm membranes; the obtained filtrates were diluted to the proper concentration range and subsequently analyzed for Hg^{2+} using a DMA-80 direct mercury analyzer and for Cd^{2+} or Pb^{2+} using a WYS2200 atomic absorption spectrophotometer.

All reagents and chemicals were of analytical grade, and all analyses were performed in triplicate.

2.3.2. Heavy Metal Sorption Capacities of the Biochars

To evaluate the heavy metal sorption ability of the biochars produced at different temperatures, the biochars produced at 300, 400, and 500 °C were tested for their Hg^{2+} , Cd^{2+} , and Pb^{2+} sorption potential in aqueous solutions. The adsorption studies were

conducted in both single and mixed solutions of the three different metal ions to explore any potential interaction effects. Specifically, the sorption experiments were carried out by mixing 0.125 g of biochar with 25 mL of heavy metal solution containing 50 mg/L Hg^{2+} , Cd^{2+} , and/or Pb^{2+} , and the mixtures were shaken for 24 h at a speed of 200 r/min under the conditions described in Section 2.3.1.

Subsequently, according to the following equation, the adsorption capacity q (mg/g) and the removal efficiency E (%) for the three heavy metals were determined by calculating the difference between the initial and final concentrations [34]:

$$q = \frac{(C_0 - C_e)V}{m}, \quad (1)$$

where q (mg/g) is the mass of metal ions adsorbed by unit biochar; C_0 and C_e (mg/L), respectively, are the metal concentrations of the initial and equilibrium experimental solution; V (L) is the volume of the heavy metal aqueous solution; and m (g) is the weight of the added biochar.

2.3.3. Isotherm Studies

Isotherm studies were performed by mixing 0.125 g of selected biochar with 25 mL of heavy metal solution containing 0.15, 0.3, 0.75, 1.5, 2.25, 3, 4.5, 6.0, 7.5, and 9.0 mmol/L Hg^{2+} , Cd^{2+} , and Pb^{2+} . In the comparative experiment with maize straw and wheat straw raw biochar, the concentrations of Hg^{2+} , Cd^{2+} , and Pb^{2+} were 0.1, 0.2, 0.5, 1, 1.5, 2, 3, 4, 5, and 6 mmol/L. The other experimental conditions were consistent with those of the sorption tests. The initial working solution concentration and the final equilibrium solution concentration of heavy metals were determined by calculating the biochars' adsorbing capacity to the different three metals. Subsequently, part of the solids in the centrifuge tubes was collected and washed with deionized water three times for FTIR and XRD to study the adsorption mechanism [35].

By fitting the data to the Langmuir and Freundlich adsorption isothermal models, the sorption capacities and binding intensities of biochar to Hg^{2+} , Cd^{2+} , and Pb^{2+} were evaluated. The Langmuir model is based on the uniform and monolayer adsorption hypothesis, whereas the Freundlich model is established on multilayer heterogeneous surface sorption. The two model equations are as follows [36]:

$$\text{Langmuir isotherm : } q_e = \frac{Q_{max}K_L C_e}{K_L + C_e} \quad (2)$$

$$\text{Freundlich isotherm : } q_e = K_F C_e^{\frac{1}{n}}, \quad (3)$$

where q_e (mg/g) is the amount of equilibrium adsorption; Q_{max} (mg/g) is the theoretical maximum sorption capacity; C_e (mg/L) is the equilibrium concentration after the adsorption experiment; K_L (mg/L) and K_F (mg/g) represent the adsorption constants of the two models, respectively; n is relevant to the heterogeneity of the adsorption point, indicating the binding intensity of sorbents [37]. These parameters can be calculated by the slope and intercept obtained by substituting the corresponding experimental data into the linearization plotting [38].

2.3.4. Kinetic Studies

Kinetic studies were conducted in 1.5 mmol/L solutions of Hg^{2+} , Cd^{2+} , and Pb^{2+} at different time intervals (5, 10, 20, and 30 min and 1, 2, 4, 6, 12, 24, 48, and 72 h). The kinetic models depict the rate of metal ions adsorbed onto biochar and illustrate the adsorption mechanism. Generally, pseudo-first-order and pseudo-second-order models are widely used in kinetic studies. According to the linear form of the equations, the parameters

were calculated by the slope and intercept obtained from plotting linearized independent variables against dependent variables [36]:

$$\text{Pseudo-first-order kinetic : } \ln(q_e - q_t) = \ln q_e - k_1 t \quad (4)$$

$$\text{Pseudo-second-order kinetic : } \frac{t}{q_t} = \frac{1}{k_2 q_e^2} + \frac{1}{q_e} t, \quad (5)$$

where q_e and q_t (mg/g) are the amounts of metal ion uptake at equilibrium and time t (min), respectively, and k_1 (min^{-1}) and k_2 (g/mg (min)) are the rate constants for the models, respectively [38].

3. Results and Discussion

3.1. Biochar Characterization

3.1.1. Fundamental Properties

Table 1 shows selected properties of BC300, BC400, and BC500. When the pyrolysis temperature increased from 300 to 500 °C, the biochar ash content increased from 21.31% to 24.54% (Table 1). As the pyrolysis temperature increased, the concentrations of minerals and the combustion residues of organic matter increased [32]. In a study by Mohammad et al. [39], the ash content of biochar increased from 4.53% to 8.64% with a temperature increase from 400 to 800 °C. The BC300 was slightly alkaline (pH = 7.49), whereas the higher production temperatures for BC400 and BC500 resulted in higher pH values (8.95 and 9.85, respectively) (Table 1). Pyrolysis temperature can affect biochar as follows: first, an increasing temperature causes the decomposition of acidic substances and promotes the formation of ash from alkali-containing minerals [40]; second, biochar produced at low temperatures may have a higher density of acidic functional groups [41]. The EC reflects the soluble salt content in biochar. The EC value of BC400 (5.74 mS/cm) was significantly higher than that of BC500 (2.79 mS/cm) (Table 1), most likely because with the increasing temperature, the alkali salt in the biomass first separated from the organic matter and then combined into a stable compound at high temperatures. Cantrell et al. showed that there is a low correlation ($0.005 < R^2 < 0.13$) between EC and ash, indicating that some elements in ash may occur in the form of water-insoluble oxides or hydroxides [42]. In this study, the surface area and pore volume of BC400 (SA = 12.110 m²/g, PV = 0.02517 cm³/g) were relatively low, whereas those of BC300 (SA = 29.598 m²/g, PV = 0.03295 cm³/g) were higher. Most likely, a higher temperature eventually leads to the loss of micropores/surface area due to pore expansion and clogging [43]. At a pyrolysis temperature of 500 °C, the organic matter burns more completely, and the pore structure of biochar becomes larger, along with an increased specific surface area [44].

Table 1. Fundamental properties of the three different biochars. EC = electrical conductivity, SA = surface area, and PV = pore volume.

Biochar	BC300	BC400	BC500
pH	7.49	8.95	9.85
EC (mS/cm)	3.22	5.74	2.79
Ash content/%	21.31	22.78	24.54
Water-soluble phosphorus (mg/kg)	477.33	596.75	233.53
SA (m ² /g)	29.598	12.110	23.303
PV (cm ³ /g)	0.03295	0.02517	0.03170

3.1.2. Elemental Analysis

Generally, the composition of biochar elements changed with the pyrolysis temperature. The H and O contents decreased from 3.792% to 2.706% and 17.838% to 8.964%, respectively, whereas the C content increased from 54.88% to 61.71% as the pyrolysis temperature increased from 300 to 500 °C (Table 2). Both the H and O contents in the biochars decreased at higher temperatures due to the dehydration of organic compounds

and the loss of volatile components [45]. Furthermore, the H/C and O/C ratios of biochars significantly decreased from 0.069 to 0.044 and 0.325 to 0.145, respectively, with increasing temperatures (Table 2). The ratios of (O+N)/C were lower in the biochars produced at 500 °C than in those produced at 300 °C, indicating that the surface of the biochars was more aromatic and less hydrophilic [41,46], most likely because of the higher degree of the carbonization of organic components and the removal of polar functional groups to form aromatic structures [47].

Table 2. Elemental analysis of the three different biochars.

Biochar	BC300	BC400	BC500
C/%	54.88	55.00	61.71
H/%	3.792	3.192	2.706
N/%	2.18	2.26	2.08
O/%	17.838	16.768	8.964
H/C	0.069	0.058	0.044
O/C	0.325	0.305	0.145
(O+N)/C	0.365	0.346	0.179

3.1.3. FTIR Analysis

Previous studies have shown that oxygen-containing functional groups can fix heavy metals [48–50]. Therefore, FTIR spectroscopy was applied to determine the variety of functional groups on the biochar surface. Figure 1 shows the FTIR spectra of the three biochars. The peak intensities of CO_3^{2-} (1430 cm^{-1}) and PO_4^{3-} (1083 cm^{-1}) increased with increasing temperatures as the water and organic matter decomposed into PO_4^{3-} - and CO_3^{2-} -associated minerals at high temperatures [32]. The peaks at 3385 and 2910 cm^{-1} , respectively, indicated phenolic-OH and methyl C = H [48,49], whose intensity first increased and then decreased with increasing temperatures, with maximum values at 400 °C . Conversely, the intensity of the peak at 1600 cm^{-1} , attributed to aromatic carbonyl/carboxyl C = O [39], increased as the pyrolysis temperature rose to 400 °C , whereas the intensity was relatively stable at 400 to 500 °C . The higher the production temperature was, the higher the intensity was of the 874 and 796 cm^{-1} (aromatic C-H vibrations) peaks [50], indicating that the higher the pyrolysis temperature was, the higher the aromaticity of the biochar was, which is in agreement with the results shown in Table 2. The types of biochar functional groups were similar at all three pyrolysis temperatures; the absorption peak of the oxygen-containing functional group of BC400 was the highest.

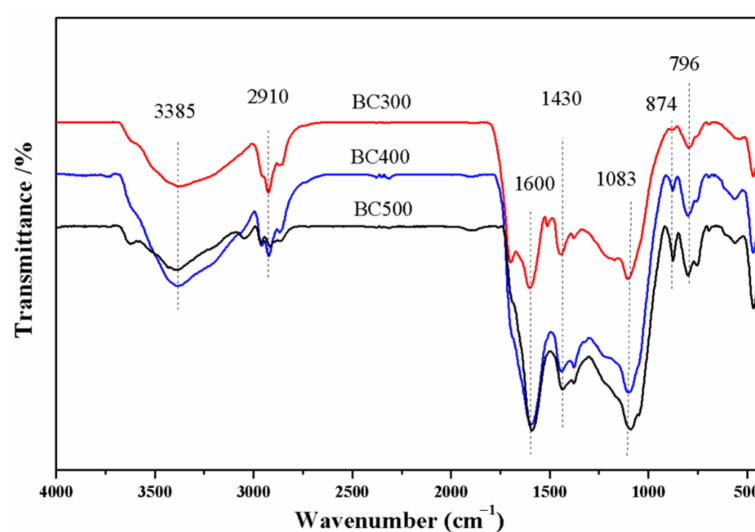


Figure 1. FTIR spectra of maize stalk biochar at temperatures of 300, 400, and 500 °C.

3.2. Adsorption Isotherms

Figure 2 shows the isotherms of the sorption of heavy metals by BC300, BC400, and BC500, described by Langmuir and Freundlich models. Biochars produced at different temperatures (BC400 > BC500 > BC300) showed similar adsorption effects for Hg^{2+} , Pb^{2+} , and Cd^{2+} ; adsorption increased dramatically when the equilibrium solution concentrations of the metals were low. With the further increase of the equilibrium metal ion concentration, the adsorption tended to be stable.

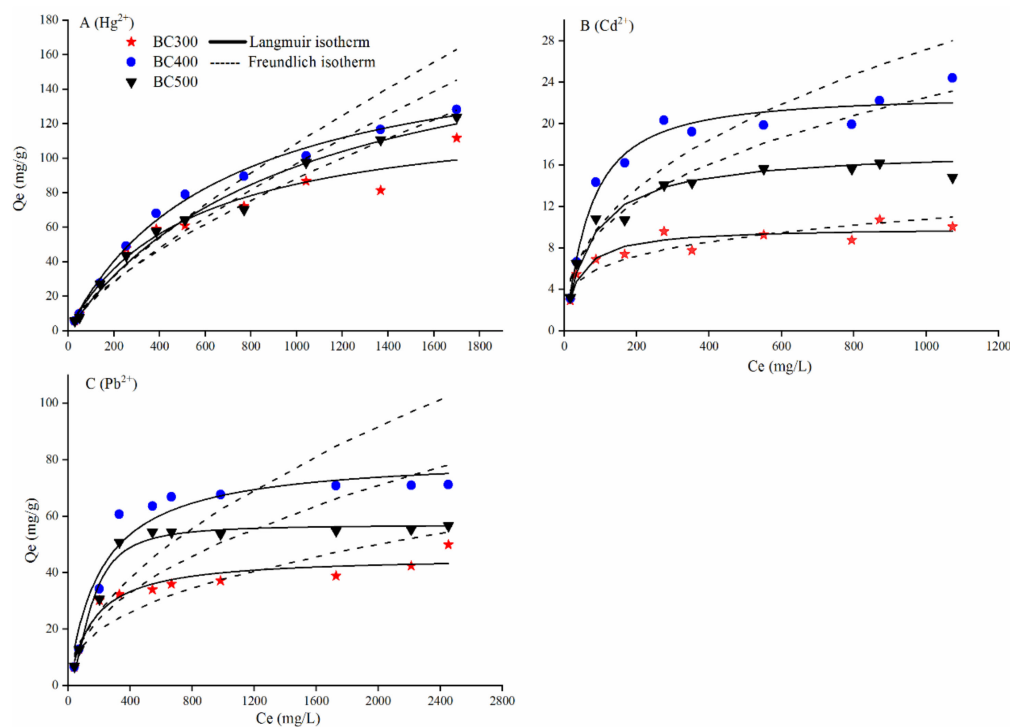


Figure 2. Isotherms of the sorption of heavy metals by BC300, BC400, and BC500, described by Langmuir and Freundlich models.

To explore the adsorption mechanism, isotherms were fitted using the Langmuir and Freundlich model equations. According to the fitting parameters (Table 3), the Langmuir model ($R^2 = 0.93\text{--}0.99$) generally showed good fit to balanced data. In particular, the Freundlich model ($R^2 = 0.95\text{--}0.97$) also well described the isothermal adsorption of Hg^{2+} . According to a previous study, the adsorption mechanism of Hg^{2+} is not only single-layer adsorption but is also accompanied by multi-layer adsorption [51]. In general, BC400 had a stronger adsorption capacity for the three heavy metals, except that the maximum adsorption capacity for Hg^{2+} of BC500 ($q_m = 190.24$ mg/g) was higher than that of BC400 ($q_m = 173.27$ mg/g). These results can be explained by the higher electrical conductivity of BC400 releasing more soluble salts into the solution and thereby strengthening the electrostatic interaction between the metal cation and the negatively charged carbon surface. In addition, the contents of functional groups and inorganic mineral components, which can form precipitates with metal ions, were higher in BC400. The presence of functional groups increases the number of adsorption sites of heavy metals, and the mineral components increase the affinity of biochar for heavy metal ions. In this study, the maize straw biochars produced at 400 °C had the highest adsorption effect for all three tested heavy metals.

Table 3. Regression parameters of Langmuir and Freundlich models for adsorption of Hg²⁺, Cd²⁺, and Pb²⁺ by biochars.

Metal Ion	Biochar	Langmuir Model			Freundlich Model		
		q _m (mg/g)	K _L (L/mg)	R ²	K _F (mg/g)	n	R ²
Hg ²⁺	BC300	129.31	0.00192	0.963	0.729	1.440	0.951
	BC400	173.27	0.00152	0.995	0.553	1.308	0.966
	BC500	190.24	0.00100	0.985	0.497	1.310	0.973
Cd ²⁺	BC300	9.27	0.02700	0.964	1.947	4.034	0.839
	BC400	22.83	0.00656	0.965	1.482	2.374	0.856
	BC500	17.59	0.02213	0.975	1.798	2.731	0.860
Pb ²⁺	BC300	45.45	0.00457	0.938	2.315	2.472	0.834
	BC400	81.47	0.00479	0.942	1.479	1.841	0.824
	BC500	56.84	0.00010	0.979	1.938	2.111	0.801

As shown in Table 3, the maximum adsorption capacities of the three biochars (BC300, BC400, and BC500) for Hg²⁺ were 129.31, 173.27, and 190.24 mg/g, respectively, whereas for Cd²⁺, they were 9.97, 22.83, and 17.59 mg/g, respectively, and for Pb²⁺, they were 45.45, 81.47, and 56.84 mg/g, respectively. These findings indicate that the three biochars have the same maximum adsorption capacity (Hg²⁺ > Pb²⁺ > Cd²⁺); for Cd²⁺, it was significantly lower than for Hg²⁺ and Pb²⁺. Consequently, maize straw biochar has a stronger affinity for Hg²⁺. There may be two mechanisms (single-layer and multi-layer adsorption) for biochar adsorption to Hg²⁺, with a stronger adsorption capacity [51,52]. Most likely, this is because as the hydrated ionic radii of metals decrease, the force of metal ion attraction to a charged surface increase. Since the ionic hydrated radius of Pb²⁺ (0.404) was lower than that of Cd²⁺ (0.426), the adsorption amount of Pb²⁺ was greater than that of Cd²⁺. The Freundlich model constant n value ranged from 1 to 10, indicating that it is beneficial to adsorption. The values of n (1 < n < 5) in Table 3 are all within this range, indicating that the three types of biochar preferentially adsorb Pb²⁺, Cd²⁺, and Hg²⁺.

3.3. Adsorption Kinetics

Figure 3 illustrates the amounts of heavy metal ions (Hg²⁺, Cd²⁺, and Pb²⁺) adsorbed by BC300, BC400, and BC500 as a function of adsorption time (0–72 h). The amounts of the three adsorbents for heavy metal ions reached equilibrium over time. In the early stage of adsorption, the biochars had high adsorption rates for the heavy metal ions, probably because adsorption mainly occurs on the outer surface of the biochar. Over time, the heavy metal ions gradually diffused into the carbon pores and further reacted with the adsorption sites inside the biochar; the adsorption rate at these sites was relatively low [52]. After 24 h of the experiment, the adsorption of metal ions by the biochars had reached equilibrium. The equilibrium adsorption capacity of metal ions for the three biochars followed the order BC400 > BC500 > BC300, which is consistent with the isothermal adsorption results.

Figure 3 shows the fitting results for the pseudo-first-order kinetic and pseudo-second-order kinetic models of the heavy metal adsorption by biochar. The experimental and theoretical calculations of adsorption balance values (q_e) and the kinetic correlation coefficients are listed in Table 4. As shown in Table 3, compared with the pseudo-second-order kinetic model (R² of 0.991–0.999), the pseudo-first-order kinetic model (R² of 0.508–0.991) had a poor fitting correlation coefficient. These results suggest that the adsorption of Hg²⁺, Cd²⁺, and Pb²⁺ by the maize straw biochars was mainly based on chemical reactions. In contrast, under the pseudo-second-order kinetic model, the results of the calculation were in good agreement with the experimental results, suggesting that this model is more suitable for describing the adsorption behavior of biochar for metal ions.

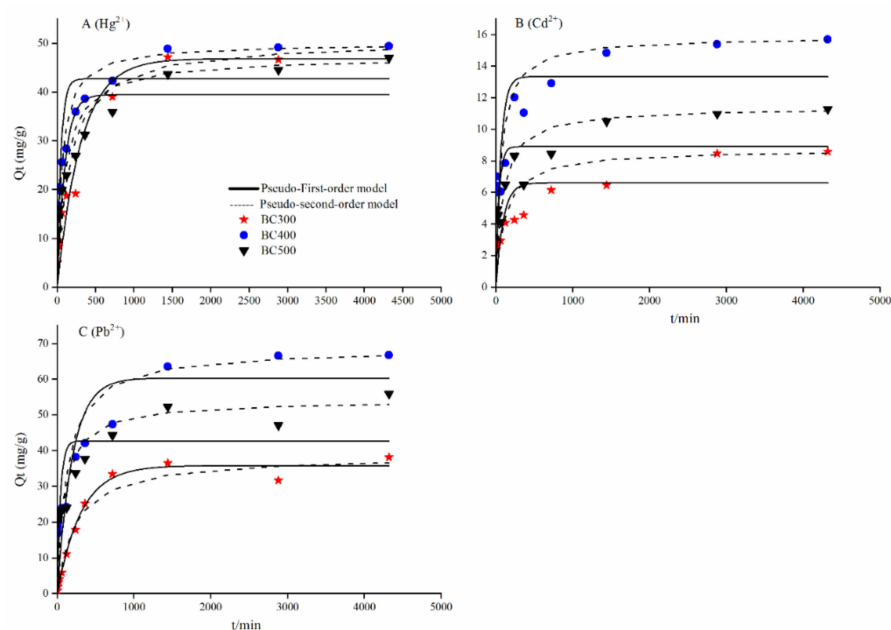


Figure 3. Sorption kinetics for Pb^{2+} , Hg^{2+} , and Cd^{2+} by maize straw biochar produced at 300, 400, and 500 °C.

Table 4. Regression parameters of pseudo-first-order and pseudo-second-order models for adsorption of Hg^{2+} , Cd^{2+} , and Pb^{2+} by the three different biochars.

Metal Ions	Biochar	Pseudo-First-Order			Pseudo-Second-Order		
		q_e (mg/g)	k_1 (min^{-1})	R^2	q_e (mg/g)	k_2 (mg/g min)	R^2
Hg^{2+}	BC300	34.10	0.001	0.820	50.51	0.0001	0.995
	BC400	28.95	0.002	0.914	50.00	0.0003	0.999
	BC500	27.98	0.001	0.892	47.17	0.0002	0.997
Cd^{2+}	BC300	6.16	0.001	0.948	8.72	0.0007	0.988
	BC400	8.20	0.001	0.945	15.87	0.0008	0.999
	BC500	6.17	0.001	0.945	11.39	0.0009	0.996
Pb^{2+}	BC300	25.12	0.001	0.508	38.61	0.0001	0.988
	BC400	51.56	0.002	0.991	68.49	0.0001	0.996
	BC500	28.41	0.001	0.600	54.05	0.00002	0.991

3.4. Sorption of Hg, Cd, or Pb by Maize Biochar Produced under Different Temperatures

Figure 4 shows the adsorption capacities of the three biochars for Hg^{2+} , Cd^{2+} , and Pb^{2+} in single- and multiple-solution systems. In the two systems, biochars showed the same affinity for the three heavy metal ions ($\text{Hg}^{2+} > \text{Pb}^{2+} > \text{Cd}^{2+}$), which was consistent with the results of the isotherm adsorption experiment. In the single-solution systems, the adsorption capacities for Hg^{2+} and Pb^{2+} of biochars produced at the three temperatures were similar, whereas that of Cd^{2+} was different; the adsorption capacities of BC300, BC400, and BC500 were 6.03, 9.11, and 7.56 mg/g, respectively.

Previous studies have shown that the main mechanisms of biochar adsorption of Cd^{2+} are cation exchange, biochar surface functional group complexation, and carbonate and phosphate precipitation [53]. Table 1 shows that the conductivity ($\text{EC} = 5.74 \text{ mS/cm}$) and water-soluble phosphorus (596.75 mg/kg) values of BC400 were greater than those of BC300 and BC500, which may explain the highest adsorption of Cd^{2+} by BC400. Although the specific surface areas of the three types of biochars were significantly different, the surface area had no significant effect on the adsorption of Pb^{2+} and Hg^{2+} , indicating that the Pb^{2+} and Cd^{2+} sorption was not controlled by the surface area. This was consistent

with the findings of a previous study in which BC400 had the lowest specific surface area but the largest adsorption capacity for Cd^{2+} [54].

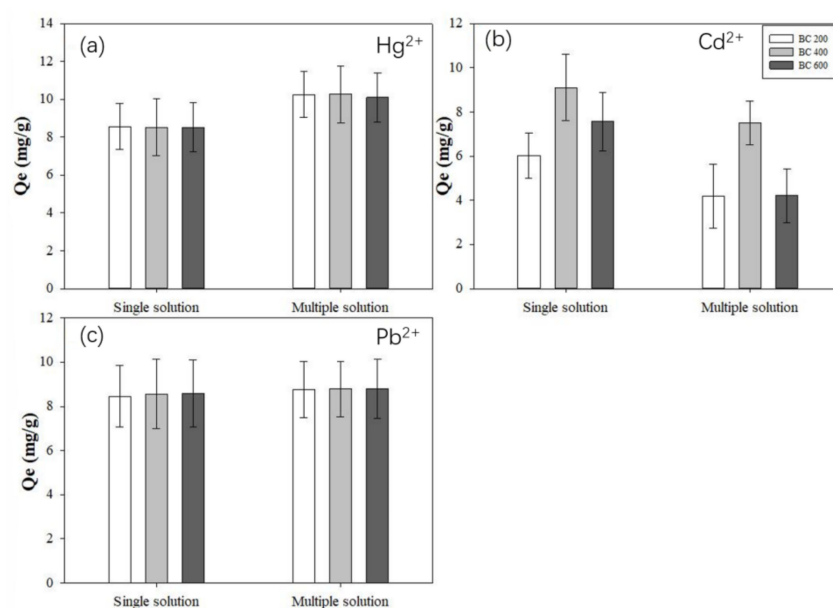


Figure 4. Adsorption capacities for (a) Hg^{2+} , (b) Cd^{2+} , and (c) Pb^{2+} of biochars in single and multiple heavy metal solution systems. The (a–c) were the adsorption capacities for Hg^{2+} , Cd^{2+} , and Pb^{2+} of biochar's, respectively.

In the multi-element system, the three heavy metals in the solution interacted with each other. The adsorption capacities for Hg^{2+} and Pb^{2+} by biochar in the multi-element system were higher than those in the single system by approximately 1.75 and 0.2 mg/g, respectively. However, the adsorption capacity of biochar for Cd^{2+} decreased, and the adsorption capacities of BC300, BC400, and BC500 decreased by 1.85, 1.61, and 3.34 mg/g, respectively. This suggests that competitive adsorption occurred when Pb^{2+} , Hg^{2+} , and Cd^{2+} coexisted in the medium. Most likely, the adsorption sites on the biochar were preferentially occupied by Pb^{2+} and Hg^{2+} [55], resulting in an inhibition of Cd^{2+} adsorption and the promotion of the adsorption and fixation of Hg^{2+} and Pb^{2+} . Since Cd^{2+} and Pb^{2+} have similar properties in aqueous solutions, they have the same adsorption mechanism [53]. However, the electronegativity of Pb^{2+} is greater, and biochar has greater affinity with it, thereby inhibiting the adsorption of Cd^{2+} by biochar. As seen in Figure 2, there were PO_4^{3-} groups on the surface of the maize straw biochars. The solubility product of the precipitate formed by Hg^{2+} was greater than those of the phosphate compounds of Cd^{2+} and Pb^{2+} , resulting in an advantage in competitive adsorption.

3.5. Comparison of BC400 and WBC400 Heavy Metal Adsorption

According to a previous study, wheat can also be used to produce biochar for the removal of heavy metal ions [56]. The adsorption characteristics of two biochars to the three heavy metals (Hg^{2+} , Pb^{2+} , Cd^{2+}) were compared through adsorption isotherm and kinetics.

The adsorption kinetics of BC400 and WBC400 are shown in Figure 5 and Table 5. The adsorption kinetics of the two biochars could be well described by the pseudo-second-order model (R^2 of 0.994–0.999). The BC400 showed a stronger adsorption capacity and adsorption rate for Hg^{2+} ; most of the Hg^{2+} (71%) was removed by BC400 within 4 h. On the contrary, WBC400 had only removed Hg^{2+} (53%) after 4 h. However, both BC400 and WBC400 showed similar Cd^{2+} adsorption characteristics. The adsorption of Cd^{2+} by the two biochars reached equilibrium after about 24 h, with adsorption efficiencies of 45%

(BC400) and 42% (WBC400). The adsorption efficiency of BC400 to Pb^{2+} reached 90% at the time of adsorption equilibrium, whereas WBC400 only removed 48% of Pb^{2+} .

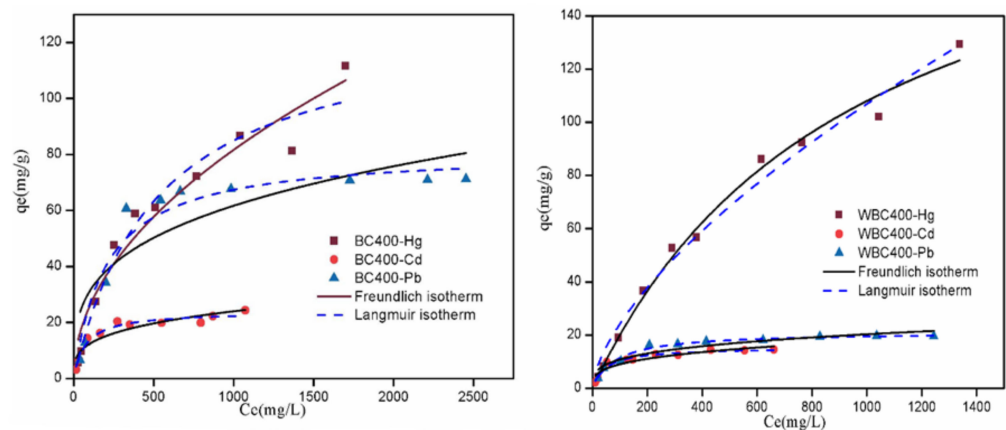


Figure 5. Sorption isotherms for three different heavy metals of BC400 and WBC400, described by Langmuir and Freundlich models.

Table 5. Regression parameters of Langmuir and Freundlich models for adsorption of Hg^{2+} , Cd^{2+} , and Pb^{2+} by BC400 and WBC400. The (A), (B) and (C) were the sorption kinetics of Hg^{2+} , Pb^{2+} and Cd^{2+} by BC400 and WBC400, respectively.

Metal Ions	Biochar	Langmuir Model			Freundlich Model		
		Q_m (mg/g)	K_L (L/mg)	R^2	K_F (mg $^{1-n}$ /(g \cdot L n))	n	R^2
Hg^{2+}	BC400	217.39	0.001	0.995	2.55	1.31	0.972
	WBC400	256.41	0.001	0.999	0.39	1.21	0.990
Pb^{2+}	BC400	128.21	0.003	0.993	1.81	1.77	0.861
	WBC400	21.88	0.011	0.981	1.72	2.71	0.887
Cd^{2+}	BC400	29.24	0.011	0.983	1.69	2.31	0.856
	WBC400	17.48	0.013	0.990	1.09	2.33	0.863

Figure 6 and Table 6 show the adsorption isotherms. For the two types of biochars, the Langmuir model showed good adaptability to equilibrium data (R^2 of 0.981–0.999), indicating that monolayer adsorption dominated. The maximum monolayer adsorption capacities of BC400 and WBC400 for Hg^{2+} and Cd^{2+} were, respectively, 217.39, 256.41, 29.24, and 17.48 mg/g. The maximum monolayer adsorption capacity of BC400 (128.21 mg/g) for Pb^{2+} was considerably higher than that of WBC400 (21.88 mg/g). After the analysis of adsorption thermodynamics and kinetics and a comprehensive comparison of the removal effects for the three heavy metals, BC400 was considered a promising biochar for removing heavy metals.

Table 6. Regression parameters of pseudo-first-order and pseudo-second-order models for adsorption of Hg^{2+} , Cd^{2+} , and Pb^{2+} by BC400 and WBC400.

Metal Ions	Biochar	Pseudo-First-Order			Pseudo-Second-Order		
		q_e (mg/g)	k_1 (min $^{-1}$)	R^2	q_e (mg/g)	k_2 (mg/g min)	R^2
Hg^{2+}	BC400	28.95	0.002	0.914	50.00	0.0003	0.999
	WBC400	23.18	0.0017	0.987	37.31	0.0002	0.998
Pb^{2+}	BC400	51.56	0.002	0.991	68.49	0.0001	0.999
	WBC400	6.20	0.0009	0.806	19.56	0.0012	0.994
Cd^{2+}	BC400	8.20	0.001	0.945	15.87	0.0008	0.996
	WBC400	6.16	0.0008	0.964	12.07	0.0008	0.995

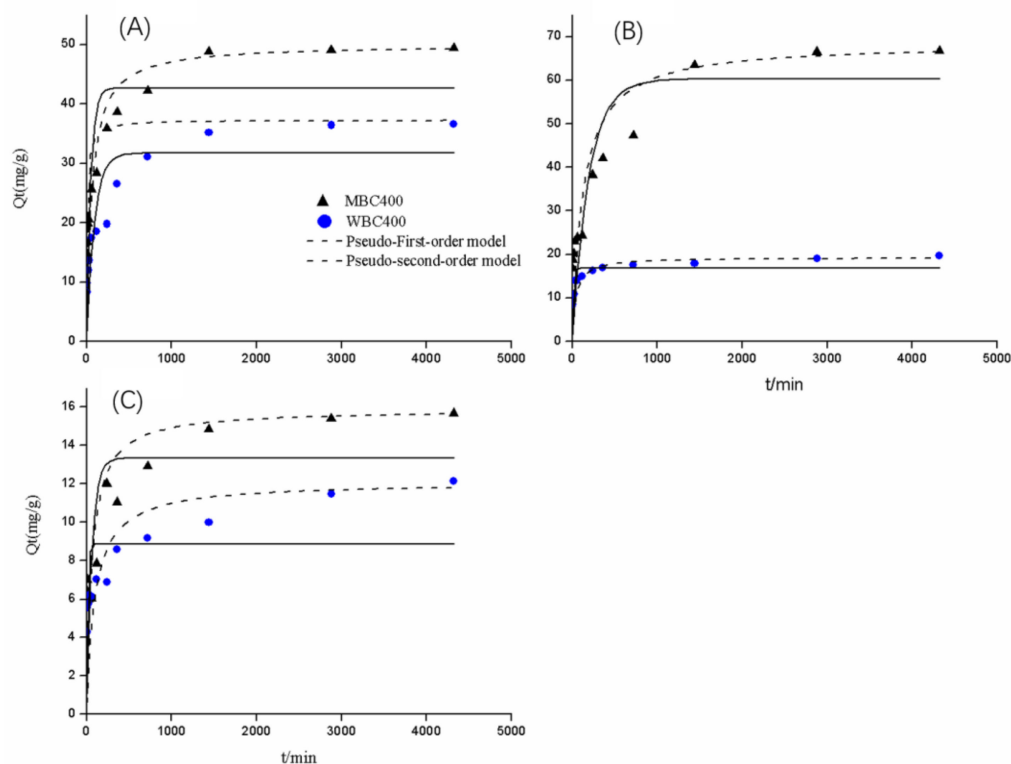


Figure 6. Sorption kinetics of, (A) Hg^{2+} , (B) Pb^{2+} and (C) Cd^{2+} by BC400 and WBC400.

3.6. BC400 Adsorption Mechanism

Of the three biochars, based on characterization, adsorption kinetics, and adsorption thermodynamic analysis, BC400 had obvious advantages. Therefore, we explored the mechanism underlying the heavy metal adsorption by BC400.

To determine the variety of functional groups involved in the heavy metal ion adsorption in solution, FTIR was applied. According to the FTIR spectra (Figure 7), the peak of $-OH$ at 3385 cm^{-1} in BC400 shifted toward 3369 , 3348 , and 3357 cm^{-1} after Pb^{2+} , Hg^{2+} , and Cd^{2+} adsorption, respectively. In addition, the intensity of the $C-H$ (2910 cm^{-1}), aromatic carbonyl/carboxyl $C=O$ (1600 cm^{-1}), and aromatic $C-H$ vibration (874 and 796 cm^{-1}) peaks weakened. These obvious peak changes indicate that heavy metal ions may have formed complexes with functional groups, caused by delocalized π electrons. The peak of PO_4^{3-} at 1099 cm^{-1} shifted to 1088 , 1087 , and 1106 cm^{-1} after heavy metal adsorption, indicating that the three heavy metal ions combined with PO_4^{3-} and formed precipitates. The peak of CO_3^{2-} (1430 cm^{-1}) weakened and slightly shifted, indicating that Pb^{2+} and Hg^{2+} combined with CO_3^{2-} and formed precipitates; however, there was no obvious change in the peak of CO_3^{2-} after BC400 had adsorbed Cd^{2+} . In a previous study, Xu et al. reported that surface $-OH$ groups, delocalized π electrons, and CO_3^{2-} or PO_4^{3-} promote the adsorption of heavy metals by biochar through precipitation and complexation [31].

To explore the effect of BC400 on the precipitation of the three heavy metal ions, BC400 was scanned by XRD after adsorption, and the spectra are presented in Figure 8. The characteristic peaks of $Pb_3(PO_4)_2$, $Hg_3(PO_4)_2$, $Cd_3(PO_4)_2$, $HgCO_3$, $PbCO_3$, $Pb(OH)_2$, $Cd(OH)_2$, and HgO occurred. Considering the high content of water-soluble phosphorus (596.75 mg/kg) in BC400 (Table 1) and the FTIR spectra indicating the significant shift due to PO_4^{3-} (Figure 7), these three heavy metal ions seemingly precipitated in the form of phosphate. Given that the characteristic peak of CO_3^{2-} weakened after Hg^{2+} and Pb^{2+} were adsorbed by BC400, they may have precipitated in the form of carbonate. In addition, Pb^{2+} and Cd^{2+} precipitated as hydroxides, and Hg^{2+} precipitated in the oxidation state.

This may be due to the unstable mercury hydroxide, directly dissolving into mercury oxide with lower solubility.

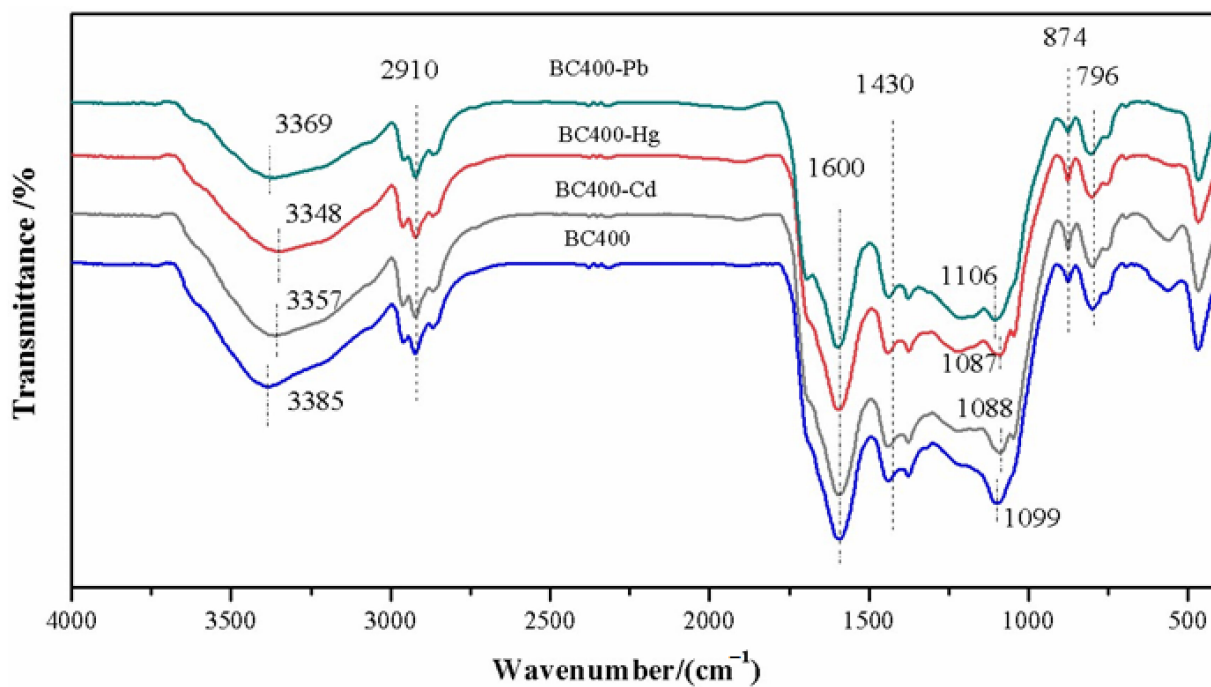


Figure 7. FTIR spectra of BC400 before and after metal sorption.

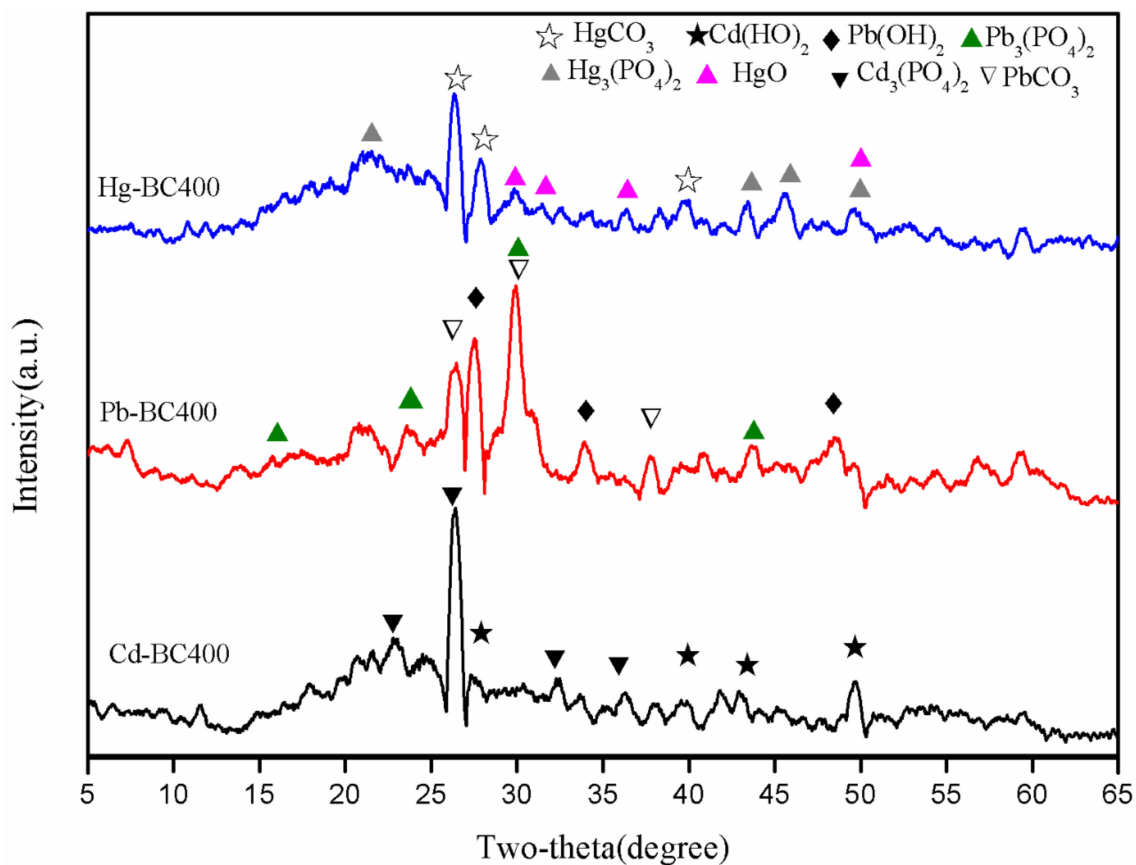


Figure 8. XRD patterns of BC400 after metal sorption.

4. Conclusions

This study investigated the removal of heavy metals in aqueous solutions by maize straw biochar and explored the underlying adsorption mechanism. Pyrolysis temperature strongly influenced the physical and chemical properties of the biochars produced from maize straw. The BC400 showed significantly higher EC values and water-soluble phosphorus contents and had more oxygen-containing functional groups, resulting in higher heavy metal removal capacities. The fitting effect of the Langmuir model was most suitable. The pseudo-second-order model was more suitable for describing the adsorption process of metal ions by biochar. The adsorption mechanisms were single-layer adsorption and chemical reaction; Hg^{2+} was also removed by multilayer adsorption. Biochar BC400 had a higher adsorption speed and a stronger adsorption capacity than WBC400. The adsorption mechanisms for Hg^{2+} and Pb^{2+} were mainly PO_4^{3-} and CO_3^{2-} precipitation, complexation with oxygenated functional groups, and delocalized π electrons. The adsorption mechanism for Cd^{2+} was similar to those of Hg^{2+} and Pb^{2+} , and its precipitation occurred mainly through the formation of phosphate. In the multi-element system, the adsorption of Cd^{2+} to BC400 was inhibited by Pb^{2+} and Hg^{2+} ; correspondingly, the adsorption capacity for Pb^{2+} and Hg^{2+} was increased. The results indicate that biochar produced at 400 °C from maize straw may provide an effective way to enhance heavy metal removal from aqueous solutions. In addition, biochar can also be used to control heavy metal pollution in wetlands and maintain the sustainable development of wetland ecosystems in the future.

Author Contributions: X.H. wrote the paper; R.Z., R.Y. and X.T. conceived and designed the experiments; B.X., H.Y. and Z.H. analyzed the data; Q.C., F.X., H.C. and J.Q. performed the experiments and collected the data. All authors have read and agreed to the published version of the manuscript.

Funding: This research was funded by the Natural Science Foundation of Anhui Province (No. 2008085MD107), the National Natural Science Foundation of China (41977135), National Key R&D Program of China (2018YFC1803100) and Key R&D Program of Anhui Province (grant numbers 1804a0802198).

Institutional Review Board Statement: Not applicable.

Informed Consent Statement: Not applicable.

Data Availability Statement: The data that support the findings of this study are available upon request from the authors.

Conflicts of Interest: The authors declare no conflict of interest.

References

1. Theologides, C.P.; Christou, A.; Costa, K.; Ioannis, K. Assessment of toxic heavy metals concentrations in soils and wild and cultivated plant species in Limni abandoned copper mining site, Cyprus. *J. Geochem. Explor.* **2017**, *178*, 6–22.
2. Duwiejua, A.B.; Cobbina, S.J.; Quainoo, A.K. Adsorption of Potentially Toxic Metals from Mono and Multi-Metal Systems Using Groundnut and Shea Nut Shell Biochars. *J. Health Pollut.* **2018**, *8*, 180602. [[CrossRef](#)] [[PubMed](#)]
3. Ajiboye, T.O.; Oyewo, O.A.; Onwudiwe, D.C. Simultaneous removal of organics and heavy metals from industrial wastewater: A review. *Chemosphere* **2021**, *262*, 128379. [[CrossRef](#)] [[PubMed](#)]
4. Uddin, M.K. A review on the adsorption of heavy metals by clay minerals, with special focus on the past decade. *Chem. Eng. J.* **2017**, *308*, 438–462. [[CrossRef](#)]
5. Wang, Q.; Cui, P.; Yang, Q. Analysis of the Cd(II) Adsorption Performance and Mechanisms by Soybean Root Biochar: Effect of Pyrolysis Temperatures. *Bull. Environ. Contam. Toxicol.* **2021**, *107*, 553–558. [[CrossRef](#)]
6. Peng, J.F.; Song, Y.H.; Yuan, P. The remediation of heavy metals contaminated sediment. *J. Hazard. Mater.* **2009**, *161*, 633–640. [[CrossRef](#)]
7. Bordoloi, N.; Goswami, R.; Kumar, M.; Katak, R. Biosorption of Co(II) from aqueous solution using algal biochar: Kinetics and isotherm studies. *Bioresour. Technol.* **2017**, *244*, 1465–1469. [[CrossRef](#)]
8. Magid, A.; Islam, M.S.; Chen, Y. Enhanced adsorption of polystyrene Nanoplastics (PSNPs) onto oxidized corncob biochar with high pyrolysis temperature. *Sci. Total Environ.* **2021**, *784*, 147115.
9. Bhuyar, P.; Farez, F.; Rahim, M. Removal of nitrogen and phosphorus from agro-industrial wastewater by using microalgae collected from coastal region of peninsular Malaysia. *Afr. J. Biol. Sci.* **2021**, *3*, 58–66. [[CrossRef](#)]

10. Bilal, M.; Ihsanullah, I.; Younas, M.; Hassan, S.M. Recent advances in applications of low-cost adsorbents for the removal of heavy metals from water: A critical review. *Sep. Purif. Technol.* **2021**, *278*, 119510. [[CrossRef](#)]
11. Chu, C.Y.; Zheng, J.L.; Chen, T.H. High Performance of Biohydrogen Production in Packed-Filter Bioreactor via Optimizing Packed-Filter Position. *Int. J. Environ. Res. Public Health* **2021**, *18*, 7462. [[CrossRef](#)]
12. Koskela, A.; Heikkil, A.; Bergna, D. Effects of Briquetting and High Pyrolysis Temperature on Hydrolysis Lignin Char Properties and Reactivity in CO-CO₂-N₂ Conditions. *Minerals* **2021**, *11*, 187. [[CrossRef](#)]
13. Wang, H.; Zhang, M.; Lv, Q. Influence of Pyrolysis Temperature on Cadmium Removal Capacity and Mechanism by Maize Straw and Platanus Leaves Biochars. *Int. J. Environ. Res. Public Health* **2019**, *16*, 845. [[CrossRef](#)]
14. Fristak, V.; Pipiska, M.; Lesny, J. Utilization of biochar sorbents for Cd(2)(+), Zn(2)(+), and Cu(2)(+) ions separation from aqueous solutions: Comparative study. *Environ. Monit. Assess.* **2015**, *187*, 4093. [[CrossRef](#)]
15. Zhang, M.; Gao, B.; Varnooosfaderani, S. Preparation and characterization of a novel magnetic biochar for arsenic removal. *Bioresour. Technol.* **2013**, *130*, 457–462. [[CrossRef](#)]
16. Park, J.H.; Choppala, G.K.; Bolan, N.S. Biochar reduces the bioavailability and phytotoxicity of heavy metals. *Plant Soil* **2011**, *348*, 439–451. [[CrossRef](#)]
17. Creamer, A.E.; Gao, B.; Zhang, M. Carbon dioxide capture using biochar produced from sugarcane bagasse and hickory wood. *Chem. Eng. J.* **2014**, *249*, 174–179. [[CrossRef](#)]
18. Li, B.; Yang, L.; Wang, C.Q. Adsorption of Cd(II) from aqueous solutions by rape straw biochar derived from different modification processes. *Chemosphere* **2017**, *175*, 332–340. [[CrossRef](#)]
19. Jiang, J.; Xu, R.K.; Jiang, T.Y.; Li, Z. Immobilization of Cu(II), Pb(II) and Cd(II) by the addition of rice straw derived biochar to a simulated polluted Ultisol. *J. Hazard. Mater.* **2012**, *229–230*, 145–150. [[CrossRef](#)]
20. Inyang, M.I.; Gao, B.; Yao, Y. A review of biochar as a low-cost adsorbent for aqueous heavy metal removal. *Crit. Rev. Environ. Sci. Technol.* **2016**, *46*, 406–433. [[CrossRef](#)]
21. Uchimiya, M.; Chang, S.; Klasson, K.T. Screening biochars for heavy metal retention in soil: Role of oxygen functional groups. *J. Hazard. Mater.* **2011**, *190*, 432–441. [[CrossRef](#)]
22. Qiu, B.; Tao, X.; Wang, H. Biochar as a low-cost adsorbent for aqueous heavy metal removal: A review. *J. Anal. Appl. Pyrolysis* **2021**, *155*, 105081. [[CrossRef](#)]
23. Uthayakumar, H.; Radhakrishnan, P.; Shanmugam, K. Growth of MWCNTs from Azadirachta indica oil for optimization of chromium(VI) removal efficiency using machine learning approach. *Environ. Sci. Pollut. Res.* **2022**, *29*, 34841–34860. [[CrossRef](#)]
24. Ahmad, M.; Rajapaksha, A.U.; Lim, J.E. Biochar as a sorbent for contaminant management in soil and water: A review. *Chemosphere* **2014**, *99*, 19–33. [[CrossRef](#)]
25. Ahmed, W.; Mehmood, S.A.; Núez, D. Enhanced adsorption of aqueous Pb(II) by modified biochar produced through pyrolysis of watermelon seeds. *Sci. Total Environ.* **2021**, *784*, 147136. [[CrossRef](#)]
26. Zhang, J.; Liu, J.; Liu, R. Effects of pyrolysis temperature and heating time on biochar obtained from the pyrolysis of straw and lignosulfonate. *Bioresour. Technol.* **2015**, *176*, 288–291. [[CrossRef](#)]
27. Fumihiko, O.M.K.; Yuka, I.; Ayaka, U.; Yuko, T.; Naohito, K. A Study on the Adsorption of Heavy Metals by Using Raw Wheat Bran Bioadsorbent in Aqueous Solution Phase. *Chem. Pharm. Bull.* **2014**, *62*, 247–253.
28. Aline, P.P.; Leónidas, C.; Azevedo, M.; Cleide, A.A. Leaching and fractionation of heavy metals in mining soils amended with biochar. *Soil Tillage Res.* **2015**, *164*, 25–33.
29. Bashir, S.; Zhu, J.; Fu, Q.; Hu, H. Cadmium mobility, uptake and anti-oxidative response of water spinach (Ipomoea Aquatic) under rice straw biochar, zeolite and rock phosphate as amendments. *Chemosphere* **2018**, *194*, 579–587. [[CrossRef](#)]
30. Fuertes, A.B.; Camps, M.; Arbestain, F. Chemical and structural properties of carbonaceous products obtained by pyrolysis and hydrothermal carbonisation of corn stover. *Aust. J. Soil Res.* **2010**, *48*, 618–626. [[CrossRef](#)]
31. Liu, Z.Q.; Zhang, H.; Jia, G.D.; Yu, X.X.; Jiang, J. Evidence of foliar water uptake in a conifer species. *Agric. Water Manag.* **2021**, *255*, 106993. [[CrossRef](#)]
32. Cao, X.; Harris, W. Properties of dairy-manure-derived biochar pertinent to its potential use in remediation. *Bioresour. Technol.* **2010**, *101*, 5222–5228. [[CrossRef](#)] [[PubMed](#)]
33. Han, L.; Sun, H.; Ro, K.S. Removal of antimony (III) and cadmium (II) from aqueous solution using animal manure-derived hydrochars and pyrochars. *Bioresour. Technol.* **2017**, *234*, 77–85. [[CrossRef](#)] [[PubMed](#)]
34. Zhou, N.; Chen, H.; Feng, Q. Effect of phosphoric acid on the surface properties and Pb(II) adsorption mechanisms of hydrochars prepared from fresh banana peels. *J. Clean. Prod.* **2017**, *165*, 221–230. [[CrossRef](#)]
35. Liu, Z.Q.; Liu, Q.Q.; Wei, Z.J.; Yu, X.X.; Jia, G.D.; Jiang, J. Partitioning tree water usage into storage and transpiration in a mixed forest. *For. Ecosyst.* **2021**, *8*, 13. [[CrossRef](#)]
36. Li, W.C.; Law, F.Y.; Chan, Y.H. Biosorption studies on copper (II) and cadmium (II) using pretreated rice straw and rice husk. *Environ. Sci. Pollut. Res. Int.* **2017**, *24*, 8903–8915. [[CrossRef](#)]
37. Venegas, A.; Rigol, A.; Vidal, M. Viability of organic wastes and biochars as amendments for the remediation of heavy metal-contaminated soils. *Chemosphere* **2015**, *119*, 190–198. [[CrossRef](#)]
38. Wang, Z. Effects of cotton straw-derived biochar under different pyrolysis conditions on Pb (II) adsorption properties in aqueous solutions. *J. Anal. Appl. Pyrolysis* **2021**, *157*, 105214. [[CrossRef](#)]

39. Al-Wabel, M.I.; Al-Omran, A.; El-Naggar, A.H. Pyrolysis temperature induced changes in characteristics and chemical composition of biochar produced from conocarpus wastes. *Bioresour. Technol.* **2013**, *131*, 374–379. [[CrossRef](#)]
40. Zhao, B.; David, O.C.; Zhang, J. Effect of pyrolysis temperature, heating rate, and residence time on rapeseed stem derived biochar. *J. Clean. Prod.* **2018**, *174*, 977–987. [[CrossRef](#)]
41. Keiluweit, M.; Nico, P.S.; Johnson, M.G. Dynamic Molecular Structure of Plant Biomass-Derived Black Carbon (Biochar). *Environ. Sci. Technol.* **2010**, *44*, 1247–1253. [[CrossRef](#)]
42. Kbc, A.; Pgh, A.; Mu, B. Impact of pyrolysis temperature and manure source on physicochemical characteristics of biochar. *Bioresour. Technol.* **2012**, *107*, 419–428.
43. Brewer, C.E.; Hall, E.T.; Schmidt, R.K. Temperature and reaction atmosphere effects on the properties of corn stover biochar. *Environ. Progress Sustain. Energy* **2016**, *36*, 696–707. [[CrossRef](#)]
44. Shen, Z.; Hou, D.; Jin, F. Effect of production temperature on lead removal mechanisms by rice straw biochars. *Sci. Total Environ.* **2019**, *655*, 751–758. [[CrossRef](#)]
45. Suliman, W.; Harsh, J.B.; AbuLail, N. Influence of feedstock source and pyrolysis temperature on biochar bulk and surface properties. *Biomass Bioenergy* **2016**, *84*, 37–48. [[CrossRef](#)]
46. Chen, X.; Chen, G.; Chen, L. Adsorption of copper and zinc by biochars produced from pyrolysis of hardwood and corn straw in aqueous solution. *Bioresour. Technol.* **2011**, *102*, 8877–8884. [[CrossRef](#)]
47. Minori, U.L. Sorption of Deisopropylatrazine on Broiler Litter Biochars. *J. Agric. Food Chem.* **2010**, *58*, 12350–12356.
48. Roscher, L.; Halbach, M.; Nguyen, M.T. Microplastics in two German wastewater treatment plants: Year-long effluent analysis with FTIR and Py-GC/MS. *Sci. Total Environ.* **2022**, *817*, 152619. [[CrossRef](#)]
49. Sun, D. Qualitative and quantitative investigation on adsorption mechanisms of Cd(II) on modified biochar derived from co-pyrolysis of straw and sodium phytate. *Sci. Total Environ.* **2022**, *829*, 154599. [[CrossRef](#)]
50. Prakash, B.; Dang, D.H.; Emelina, M.; Mohd, H.A.; Rahim, G.P.M.; Natanamurugaraj, G. Desalination of Polymer and Chemical industrial wastewater by using green photosynthetic microalgae, *Chlorella* sp. *Maejo Int. J. Energy Environ. Commun.* **2019**, *1*, 9–19. [[CrossRef](#)]
51. Liang, L.; Li, X.; Guo, Y. The removal of heavy metal cations by sulfidated nanoscale zero-valent iron (S-nZVI): The reaction mechanisms and the role of sulfur. *J. Hazard. Mater.* **2021**, *404*, 124057. [[CrossRef](#)]
52. Soares, M.B.; Milori, D.; Alleoni, L. How does the biochar of sugarcane straw pyrolysis temperature change arsenic and lead availabilities and the activity of the microorganisms in a contaminated sediment? *J. Soils Sediments* **2021**, *21*, 3185–3200. [[CrossRef](#)]
53. Li, H.; Dong, X.; Silva, E. Mechanisms of metal sorption by biochars: Biochar characteristics and modifications. *Chemosphere* **2017**, *178*, 466–478. [[CrossRef](#)]
54. Geleto, M.A.; Forján, R.; Arco-Lázaro, E. Influence of pyrolysis temperature and feedstock biomass on Cu²⁺, Pb²⁺, and Zn²⁺ sorption capacity of biochar. *Int. J. Environ. Sci. Technol.* **2022**, 1–10. [[CrossRef](#)]
55. Park, J.H.; Ok, Y.S.; Kim, S.H. Competitive adsorption of heavy metals onto sesame straw biochar in aqueous solutions. *Chemosphere* **2016**, *142*, 77–83. [[CrossRef](#)]
56. Alalwan, H.A.; Kadhom, M.A.; Alminshid, A.H. Removal of heavy metals from wastewater using agricultural byproducts. *J. Water. Supply Res. Technol.-Aqua* **2020**, *69*, 99–112. [[CrossRef](#)]